

Split Peas in a Pod: Intra-System Uniformity of Super-Earths and Sub-Neptunes

SARAH C. MILLHOLLAND^{1,*} AND JOSHUA N. WINN¹

¹*Department of Astrophysical Sciences, Princeton University, 4 Ivy Lane, Princeton, NJ 08544, USA*

ABSTRACT

The planets within compact multi-planet systems tend to have similar sizes, masses, and orbital period ratios, like “peas in a pod”. This pattern was detected when considering planets with radii between 1 and 4 R_{\oplus} . However, these same planets show a bimodal radius distribution, with few planets between 1.5 and 2 R_{\oplus} . The smaller “super-Earths” are consistent with being stripped rocky cores, while the larger “sub-Neptunes” likely have gaseous H/He envelopes. Given these distinct structures, it is worthwhile to test for intra-system uniformity separately within each category of planets. Here, we find that the tendency for intra-system uniformity is twice as strong when considering planets within the same size category than it is when combining all planets together. The sub-Neptunes tend to be $1.7^{+0.6}_{-0.3}$ times larger than the super-Earths in the same system, corresponding to an envelope mass fraction of about 2.6% for a 5 M_{\oplus} planet. For the sub-Neptunes, the low-metallicity stars are found to have planets with more equal sizes, with modest statistical significance ($p \sim 0.005$). There is also a modest ($\sim 2\text{-}\sigma$) tendency for wider-orbiting planets to be larger, even within the same size category.

1. INTRODUCTION

The NASA Kepler mission found hundreds of multiple-planet systems in which the orbital periods are all shorter than 100 days and the planets’ sizes are in between those of Earth and Neptune (Lissauer et al. 2011, 2014; Rowe et al. 2014; Fabrycky et al. 2014). Within a given system, the sizes, masses, and orbital period ratios of the planets tend to be more alike than the properties of planets drawn from different systems (Weiss et al. 2018; Millholland et al. 2017). These intra-system regularities have been nicknamed the “peas-in-a-pod pattern” (see the forthcoming review by Weiss et al. 2021). At nearly the same time, it was recognized that the radius distribution of these planets is bimodal, with few planets having sizes between 1.5 and 2 R_{\oplus} (Fulton et al. 2017; Van Eylen et al. 2018; Fulton & Petigura 2018). This so-called “radius valley” had been predicted in planetary atmosphere models (Owen & Wu 2013; Lopez & Fortney 2013; Jin et al. 2014) as an effect of photoevaporation, which turns out to be a threshold process leading either to a “super-Earth” completely stripped of its gaseous envelope or a “sub-

Neptune” with enough gas to inflate its transit radius by about a factor of two. Another possibility for these two distinct planet categories is atmospheric loss due to the heat of formation of the solid core (Ginzburg et al. 2018; Gupta & Schlichting 2019, 2020).

At first glance, these observations appear to be contradictory. Can these systems really be considered peas in a pod when their constituent planets fall into two disparate categories? One possible resolution is that a given star tends to host either mostly super-Earths or mostly sub-Neptunes; however, this is only partially the case, as demonstrated below. We have found that another important part of the resolution is that the intra-system size uniformity within each planet category is so strong that it can be detected even when the two categories are combined together before performing statistical tests. In this sense, intra-system uniformity has been underestimated in previous studies. Although super-Earths and sub-Neptunes might originate from the same initial population of gas-enshrouded rocky planets (Owen & Wu 2017; Berger et al. 2020a; Rogers & Owen 2021), today they have distinct physical structures. In this Letter, we take advantage of our knowledge of these differing structures to revisit the issue of intra-system uniformity within individual planetary categories.

sarah.milholland@princeton.edu

* NASA Sagan Fellow

2. PLANET SAMPLE

We begin with the Kepler planet sample constructed by Berger et al. (2020a), which was based on cross-matching the Kepler Object of Interest (KOI) catalog from the NASA Exoplanet Archive with the Gaia-Kepler Stellar Properties Catalog of Berger et al. (2020b). The stellar parameters were homogeneously derived using isochrones and broadband photometry, Gaia Data Release 2 parallaxes (Gaia Collaboration et al. 2018), and spectroscopic metallicities whenever they were available. After a series of quality cuts, the sample consisted of 2956 stars hosting 3898 planets. The median fractional uncertainty in the planet radius is 7%.

We consider only planets smaller than $16 R_{\oplus}$ with orbital periods shorter than 300 days. We also apply some additional quality cuts. To avoid large systematic errors in planet radii, we discard stars for which Furlan et al. (2017) found a companion star that contributed more than 5% of the light in the Kepler photometric aperture. We remove planets with fractional radius uncertainties greater than 50%. Following the advice of Petigura (2020), we omit planets for which the transit duration T was shorter than half of the maximum possible transit duration for a circular orbit,

$$T_0 \equiv \left[\frac{3}{\pi^2 G} \frac{P}{\rho_{\star}} \right]^{1/3} = 13 \text{ hr} \left(\frac{P}{\text{yr}} \right)^{1/3} \left(\frac{\rho_{\star}}{\rho_{\odot}} \right)^{-1/3}. \quad (1)$$

This is because low values of T/T_0 usually imply nearly-grazing transits for which the planet radius is especially uncertain. Finally, we remove planets for which the calculated transit signal-to-noise ratio (SNR) was less than 7.¹ The SNR is calculated as (Christiansen et al. 2012)

$$\text{SNR} = \frac{(R_p/R_{\star})^2}{\text{CDPP}_{\text{eff}}} \sqrt{\frac{t_{\text{obs}} f_0}{P}}, \quad (2)$$

where t_{obs} is the time interval over which data were collected (~ 4 years in most cases), f_0 is the duty cycle, and CDPP_{eff} is the effective combined differential photometric precision,

$$\text{CDPP}_{\text{eff}} = \text{CDPP}_{6 \text{ hr}} \sqrt{\frac{6 \text{ hr}}{T}}. \quad (3)$$

For each target star, we obtained t_{obs} , f_0 , and $\text{CDPP}_{6 \text{ hr}}$ from the Kepler Q1-Q17 stellar properties catalog (Mathur et al. 2017). Our final sample contains 2111

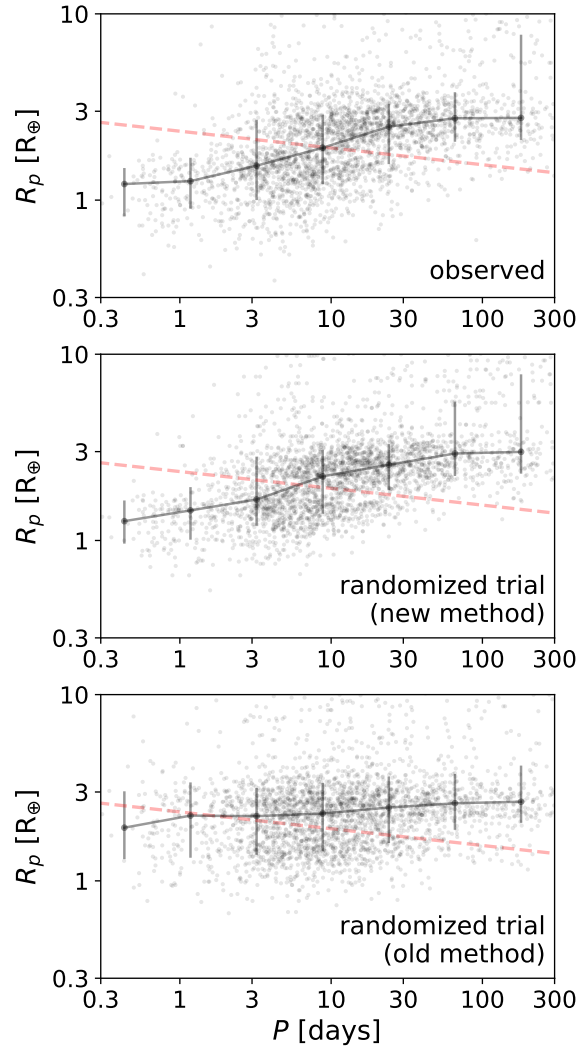


Figure 1. Planet sample in period-radius (P - R_p) space. Top panel: The observed planet sample described in Section 2. Middle panel: One randomized trial of the population using our randomization procedure intended to preserve structure in P - R_p space (the radius valley and the sub-Neptune desert). Bottom panel: One randomized trial of the population using a procedure that assigns radii independently from periods. In all panels, the red line is the radius valley boundary derived by Van Eylen et al. (2018), and the black line represents the median and 16th and 84th percentiles of the radius within logarithmic bins of period.

stars hosting 2883 planets, with 520 of the systems hosting two or more planets. Figure 1 (top panel) shows the orbital periods and planet radii.

¹ To verify that these cuts do not introduce biases, we repeated all calculations in the paper using weaker thresholds, $T/T_0 > 0.2$ (rather than $T/T_0 > 0.5$) and $\text{SNR} > 5$ (rather than $\text{SNR} > 7$). We find very similar results for all calculations, and the major findings are unchanged.

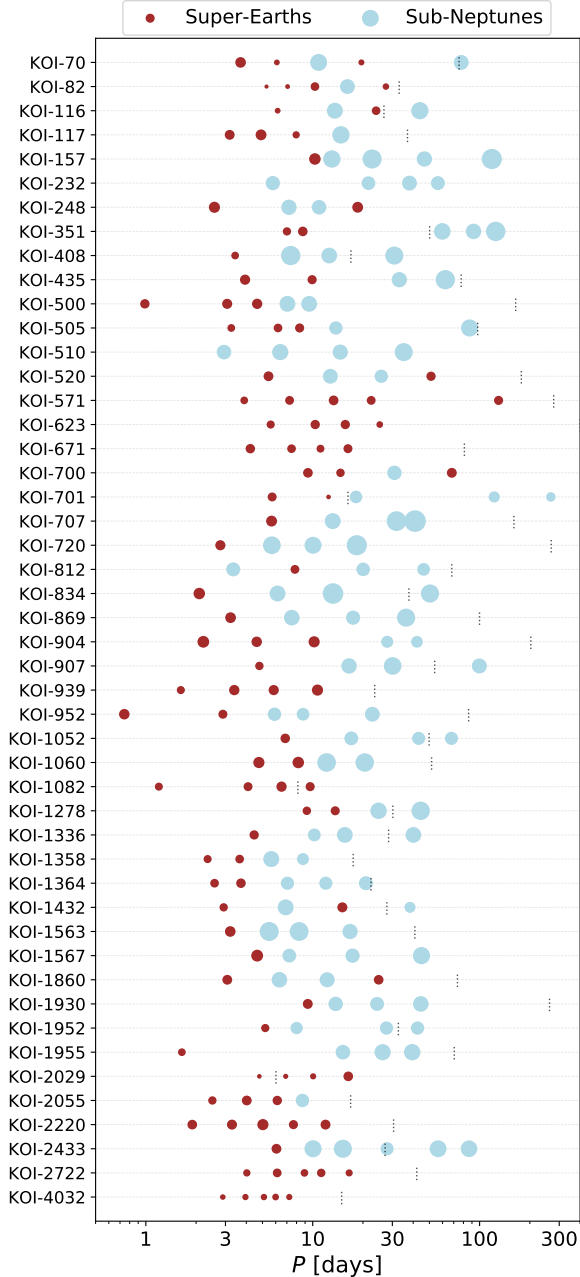


Figure 2. Architectures of systems with four or more transiting planets smaller than $4 R_{\oplus}$. The dot size is proportional to the planet radius, with super-Earths in brown and sub-Neptunes in blue. The thin vertical lines indicate the maximum orbital period for which the smallest planet in the system could have been detected with a SNR exceeding the threshold of 7. (No vertical line was drawn when this maximum period was more than 300 days.)

3. PEAS-IN-A-POD AND THE RADIUS VALLEY

We categorize a given planet as either a super-Earth (SE) or a sub-Neptune (SN) based on whether its radius is smaller or larger than the boundary of the valley in

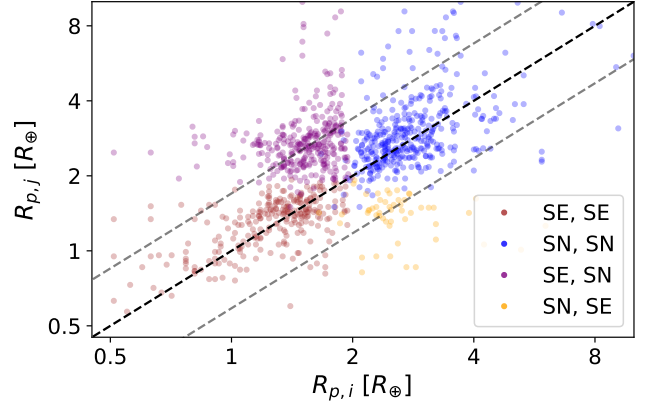


Figure 3. Radii of pairs of planets within the same system, $R_{p,j}$ vs. $R_{p,i}$ where $P_i < P_j$, including non-adjacent pairs. The color of each point conveys the size category of each planet in the pair. The dark dashed line is where $R_{p,j} = R_{p,i}$, and the lighter dashed lines are where $R_{p,j}$ is either $1.7 R_{p,i}$ or $R_{p,i}/1.7$.

P - R_p space, as defined by Van Eylen et al. (2018),

$$\log_{10}(R_p/R_{\oplus}) = m \log_{10}(P/\text{days}) + a, \quad (4)$$

with $m = -0.09^{+0.02}_{-0.04}$ and $a = 0.37^{+0.04}_{-0.02}$. Of the 2883 planets, 1265 are SEs and 1618 are SNs. Of the 520 multi-planet systems, 118 contain only SEs, 155 contain only SNs, and 247 (roughly half) contain both SEs and SNs. Figure 2 illustrates the orbital spacings and sizes for the 48 systems with at least four transiting planets smaller than $4 R_{\oplus}$. This subset is small enough to fit into a single plot, although our subsequent analysis includes all of the multi-planet systems.

Visual inspection of Figure 2 gives the impression that intra-system uniformity of planet sizes is much stronger for planets within the same size class (i.e., considering only points of the same color). A striking example is KOI-1060 (Kepler-758), which has a pair of SEs with radii $1.82 R_{\oplus}$ and $1.87 R_{\oplus}$, and a pair of SNs with radii $3.19 R_{\oplus}$ and $3.16 R_{\oplus}$.

For a quantitative analysis, we consider ratios between the radii of pairs of planets in the same system, $R_{p,j}$ vs. $R_{p,i}$ where $P_i < P_j$. To reduce asymmetries due to detection bias, we only include a planet pair in the set of radius ratios if it passes a “swap test”, wherein both planets would still be detectable if they swapped periods (Weiss et al. 2018). In practice, this requires that the inner planet must still be detectable when assigned the longer period, $\text{SNR}_i(P_i/P_j)^{1/3} > 7$. Figure 3 shows the radii of pairs of planets within the same system, including non-adjacent pairs. The points are colored by the four possible period-ordered types of pairs: (1) SE, SE; (2) SN, SN; (3) SE, SN; and (4) SN, SE. The count

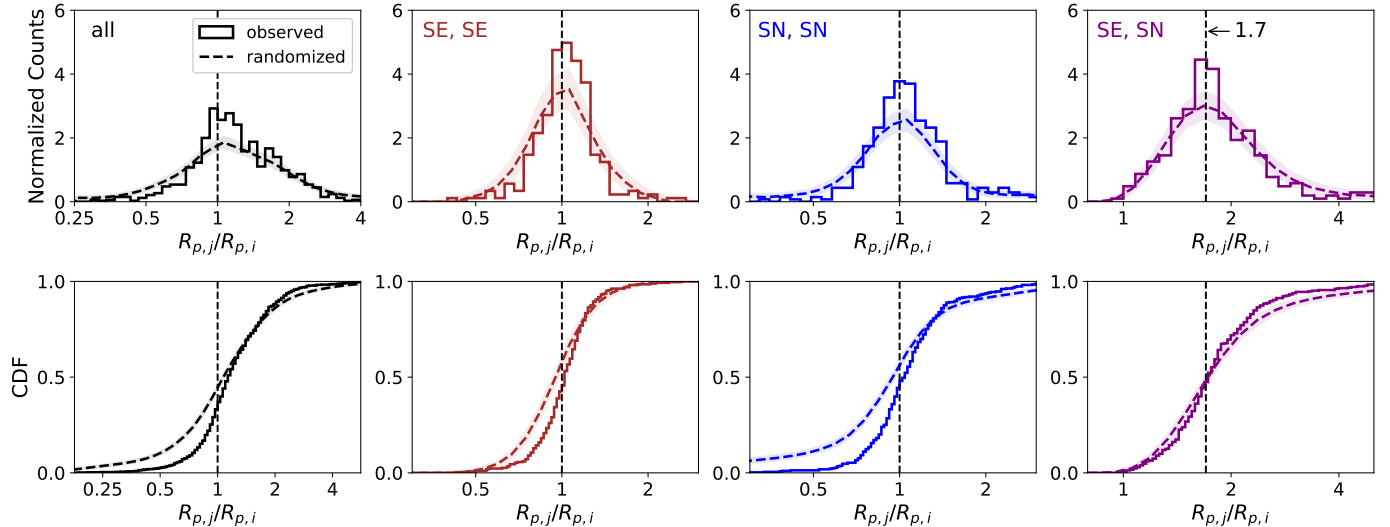


Figure 4. Normalized histograms (top panels) and cumulative distributions (bottom panels) of the radius ratios of pairs of planets within the same system, $R_{p,j}/R_{p,i}$ where $P_i < P_j$. The distributions are split by pair type, with the columns corresponding to (1) all pairs; (2) SE, SE; (3) SN, SN; and (4) SE, SN from left to right. The solid line corresponds to the observed data, while the dashed line and banding correspond to the median and 16th and 84th percentiles of the randomized trials.

and fraction of the four pair types are 265 (26%), 379 (38%), 310 (31%), and 52 (5%), respectively. Thus, for 64% of planet pairs, both planets are within the same size class, which helps to explain why intra-system uniformity was detectable in previous studies that did not split the planets into two categories.

As expected, Figure 3 shows that the SE, SE and SN, SN pairs are much more clustered along the identity line – indicating more uniform radii – than the distribution as a whole. This is an inevitable consequence of restricting the size range of the planets before performing the comparisons. More interesting is the quantification of the strength of the uniformity relative to the expectation of the null hypothesis, in which the radius ratios have the same distribution as would be obtained by drawing planets at random from the population (Millholland et al. 2017; Weiss et al. 2018; Weiss & Petigura 2020).

Null hypothesis testing is crucial because it indicates whether the uniformity trends are physical or the result of detection biases. Recently, there have been conflicting interpretations about the role of detection biases in sculpting the peas-in-a-pod patterns as a whole (Zhu 2020; Murchikova & Tremaine 2020). However, comprehensive forward models (e.g. He et al. 2019, 2020) and population synthesis models (e.g. Mishra et al. 2021) that account for detection biases find strong evidence for intra-system uniformity within the Kepler planet population. (See also Weiss & Petigura 2020.) In the next section, we apply a simple model of transit detectabil-

ity to evaluate planetary category-specific intra-system uniformity relative to random expectation.

3.1. Significance assessment using randomized trials

In previous studies of intra-system uniformity, Weiss et al. (2018) and Millholland et al. (2017) constructed the random samples necessary for the null hypothesis testing by preserving the periods and multiplicities of each system but drawing the radii at random (with replacement) from the sample’s entire distribution of planet radii. A drawback of this approach is that it does not preserve two prominent structures that are observed in P – R_p space: the radius valley and the sub-Neptune desert (the paucity of sub-Neptunes in short-period orbits). Thus, some of the random systems are unlike any real system. Moreover, erasing the structure in P – R_p space would lead to an overestimate of the strength of intra-system uniformity because the randomized systems would include SNs interior to SEs, a pattern which is rare in reality.

We devised a procedure intended to preserve the important structures in P – R_p space:

1. Within each system, for each planet with radius $R_{p,i}$ and period P_i , draw a random radius $R_{p,i,\text{rand}}$ from the subset of the full distribution with $|\log_{10} P - \log_{10} P_i| < 0.25$ (with P in days).
2. Calculate the SNR for the newly drawn planet, $\text{SNR}_{i,\text{rand}} = \text{SNR}_i(R_{p,i,\text{rand}}/R_{p,i})^2$. If $\text{SNR}_{i,\text{rand}} < 7$, redraw $R_{p,i,\text{rand}}$ and repeat.

Table 1. Significance of intra-system radius uniformity and size ordering.

	Pearson r of $R_{p,j}$ vs. $R_{p,i}$			MAD of $R_{p,j}/R_{p,i}$ distribution			fraction above $R_{p,j}/R_{p,i} = 1$		
	observed	randomized	significance	observed	randomized	significance	observed	randomized	significance
all pairs	0.444	0.030 ± 0.033	12.7σ	0.417	0.593 ± 0.028	-6.2σ	0.660	0.596 ± 0.016	4.0σ
SE, SE	0.570	0.074 ± 0.086	5.8σ	0.194	0.258 ± 0.027	-2.4σ	0.558	0.499 ± 0.041	1.5σ
SN, SN	0.383	0.002 ± 0.048	7.9σ	0.264	0.375 ± 0.027	-4.1σ	0.549	0.497 ± 0.025	2.1σ
SE, SN	0.103	-0.011 ± 0.063	1.8σ	0.432	0.569 ± 0.052	-2.6σ	–	–	–

3. When computing radius ratios $R_{p,j,\text{rand}}/R_{p,i,\text{rand}}$ for pairs of planets in the same system, check whether the pair passes the swap test: $\text{SNR}_{i,\text{rand}}(P_i/P_j)^{1/3} > 7$. Otherwise, discard the radius ratio.

Using this procedure we created 1000 synthetic populations and corresponding distributions of radius ratios. Figure 1 shows representative examples of P - R_p diagrams of synthetic populations using the old and new methods.

Figure 4 shows the radius ratio distributions of the observed and synthetic populations. We highlight three findings:

(1) *Size uniformity.* All four observed distributions are more sharply peaked around the median than the distributions based on the synthetic systems. Table 1 gives two measures of the statistical significance of intra-system uniformity: the Pearson r correlation coefficient between $R_{p,i}$ and $R_{p,j}$ (see Figure 3) and the median absolute deviation from the median (MAD) of the $R_{p,j}/R_{p,i}$ distribution. The MAD quantifies the *degree* of radius uniformity, which is about twice as strong for the SE, SE and SN, SN pairs than for all pairs (the MAD for the SE, SE and SN, SN pairs is ~ 0.2 compared to ~ 0.4 for all pairs). However, the *significance* of the uniformity relative to the randomized trials is weaker for the SE, SE and SN, SN pairs because the comparisons are made within restricted radius ranges.

(2) *Size ordering.* One might expect longer-period planets to be larger on average because planets in wider orbits are more likely to retain their atmospheres. Previous work has shown evidence for this effect in the overall planet population (Ciardi et al. 2013; Millholland et al. 2017; Kipping 2018; Weiss et al. 2018). We can now check whether size ordering is also observed for the rocky cores and gas-enveloped planets. The CDFs of the SE, SE and SN, SN pairs in the bottom row of Figure 4 show only tentative evidence of size ordering; the observed distributions appear to be shifted to the right of the randomized distributions. Table 1 gives the fraction of the radius ratio distribution for which $R_{p,j}/R_{p,i} > 1$. For the SE, SE pairs, 56% of the distribution has the larger planets on the outside, which is 1.5σ more than

in the randomized trials. For the SN, SN pairs, the corresponding numbers are 55% and 2.1σ .

(3) *Peak at $R_{p,\text{SN}}/R_{p,\text{SE}} \approx 1.7$.* The median of the SE, SN radius ratio distribution occurs at $1.7^{+0.6}_{-0.3}$ (where the lower and upper ranges indicate 16th and 84th percentiles). This seems to be telling us that $R_p/R_{\text{core}} \approx 1.7$, based on a simple physical argument. First, we expect $M_p \approx M_{\text{core}}$ because structural models show that the H/He dominated atmospheres of SNs constitute only a few percent of the planet’s total mass (Rogers 2015; Wolfgang & Lopez 2015). Further assuming that intra-system uniformity generally applies to planet mass as well as radius (Millholland et al. 2017), the uniformity in M_p implies uniformity in M_{core} , which in turn requires uniformity in R_{core} if the core compositions are similar in a given system. In this interpretation, SEs and SNs in the same system have approximately the same core size, and the characteristic radius ratio of 1.7 reflects the typical amount of gas of SNs. We will return to this point in Section 5.

4. STELLAR METALLICITY DEPENDENCE

Previous work has shown that intra-system radius uniformity depends only weakly on stellar properties. Millholland et al. (2017) performed a multiple regression between planetary system characteristics and stellar properties and showed that the variation in metallicity [Fe/H] can explain only $\approx 20\%$ of the variation of system-wide median planet sizes. Likewise, the variation in [Fe/H] could account for only $\approx 10\%$ of intra-system size dispersion. To see whether these conclusions change when the planets are separated into distinct physical categories, we considered a metric for the intra-system fractional radius dispersion (Weiss et al. 2021),

$$\sigma_{\mathcal{R}}^2 = \text{Variance} \{ \log_{10}(R_{p,j}/R_{\oplus}) \}, \quad (5)$$

where $j = 1, 2, \dots, N$ is indexed over planets in the system. We calculated $\sigma_{\mathcal{R}}$ for the SE sub-systems and the SN sub-systems and searched for any dependence on [Fe/H]. Figure 5 shows the results.

For the SE sub-systems, the Anderson-Darling test does not rule out the null hypothesis that the [Fe/H] < 0 and [Fe/H] > 0 sub-systems have the same distribution

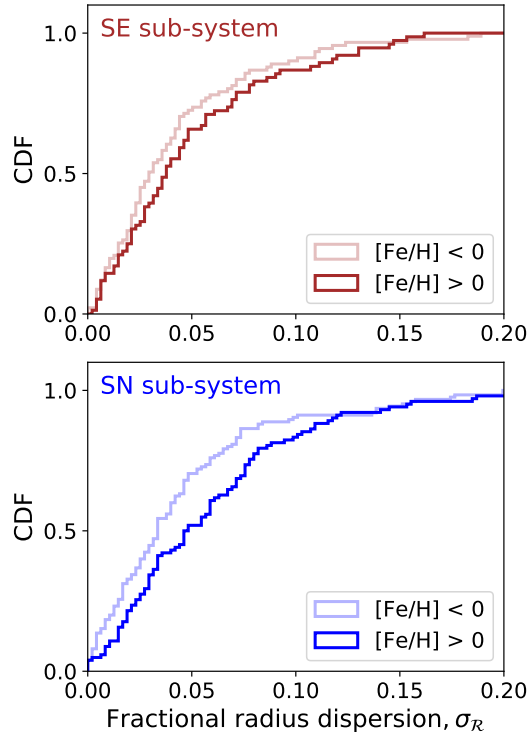


Figure 5. Cumulative distributions of the fractional radius dispersion metric, split by size class and stellar metallicity. The top (bottom) panels corresponds to $\sigma_{\mathcal{R}}$ calculated for the subset of the planets in a system in the SE (SN) size class. The lighter line colors correspond to systems with sub-solar metallicity, whereas the darker lines correspond to super-solar metallicity.

of $\sigma_{\mathcal{R}}$. For the SN sub-systems, though, the p -value is 0.005. Low-metallicity stars show slightly more uniformity in the sizes of their SNs than high-metallicity stars. This result agrees with the finding by Millholland et al. (2017) based on the concatenation of all planet types; we have shown here that the effect is more important for the SNs than for the SEs.

5. SUMMARY AND DISCUSSION

Using a large sample of Kepler systems, we have explored the “peas-in-a-pod pattern” after splitting the “peas” into two physically distinct types of planets: super-Earths (SEs) and sub-Neptunes (SNs). The radius uniformity observed within SE, SE and SN, SN pairs is about twice as strong as one would infer without splitting the planets into these two categories. The MAD of the distribution of radius ratios ($R_{p,j}/R_{p,i}$ where $P_i < P_j$) for the SE, SE and SN, SN pairs is ≈ 0.2 (Table 1), corresponding to a standard deviation of ≈ 0.3 . Thus, to a reasonable approximation, $R_{p,j}/R_{p,i} \sim \mathcal{N}(\mu = 1, \sigma = 0.3)$. For SNs, the uniformity

appears to be slightly enhanced for systems with lower stellar metallicity.

While radius uniformity is the dominant trend, there is $\sim 2\text{-}\sigma$ evidence for size ordering even when considering only SE, SE pairs or SN, SN pairs. Size ordering of the planetary systems as a whole can be readily attributed to atmospheric loss for the highly irradiated planets (e.g. Lopez & Fortney 2013) (i.e., SEs tend to be interior to SNs), but size ordering within each planet category may require a separate explanation.

In systems with both types of planets, the SN tends to be $1.7^{+0.6}_{-0.3}$ times larger than the SE. We argued that this implies $R_p \approx 1.7 R_{\text{core}}$ for sub-Neptunes. The radius fitting formula from Millholland (2019) (see also Lopez & Fortney 2014; Chen & Rogers 2016) indicates that $R_p/R_{\text{core}} \approx 1.7$ corresponds to an envelope mass fraction ($f_{\text{env}} \equiv M_{\text{env}}/M_p$) of $f_{\text{env}} \approx 4.9\%$ for $M_p \approx 10 M_{\oplus}$ and $f_{\text{env}} \approx 2.6\%$ for $M_p \approx 5 M_{\oplus}$. The observation that $R_p \approx 1.7 R_{\text{core}}$ is broadly consistent with both photo-evaporation (e.g. Owen & Wu 2017) and core-powered mass loss models (e.g. Gupta & Schlichting 2019) and seems unlikely to help distinguish between them; however, this would benefit from further study.

Theoretical investigations of intra-system uniformity suggest that it can be explained by system-to-system variations in protoplanetary disk properties, combined with characteristic mass scales that emerge during planet conglomeration processes such as pebble accretion (Weiss et al. 2021; Mishra et al. 2021). The mass scales depend on factors such as the disk scale height, solid surface density, and disk lifetime, thus yielding small variations within systems compared to those between systems. Adams (2019) have also presented a simple model of planet formation, based on an energy optimization criterion, in which uniform planet masses are the natural outcome. However, it is still unclear how specific aspects of the planet formation process map onto the quantitative *degree* of uniformity that is observed. We hope our results will be useful for future work that aims to understand the origins of both intra-system uniformity and diversity.

6. ACKNOWLEDGEMENTS

We thank the anonymous referee for their constructive comments, which helped improved this paper. S.C.M. was supported by NASA through the NASA Hubble Fellowship grant #HST-HF2-51465 awarded by the Space Telescope Science Institute, which is operated by the Association of Universities for Research in Astronomy, Inc., for NASA, under contract NAS5-26555.

REFERENCES

- Adams, F. C. 2019, *MNRAS*, 488, 1446, doi: [10.1093/mnras/stz1832](https://doi.org/10.1093/mnras/stz1832)
- Berger, T. A., Huber, D., Gaidos, E., van Saders, J. L., & Weiss, L. M. 2020a, *AJ*, 160, 108, doi: [10.3847/1538-3881/aba18a](https://doi.org/10.3847/1538-3881/aba18a)
- Berger, T. A., Huber, D., van Saders, J. L., et al. 2020b, *AJ*, 159, 280, doi: [10.3847/1538-3881/159/6/280](https://doi.org/10.3847/1538-3881/159/6/280)
- Chen, H., & Rogers, L. A. 2016, *ApJ*, 831, 180, doi: [10.3847/0004-637X/831/2/180](https://doi.org/10.3847/0004-637X/831/2/180)
- Christiansen, J. L., Jenkins, J. M., Caldwell, D. A., et al. 2012, *PASP*, 124, 1279, doi: [10.1086/668847](https://doi.org/10.1086/668847)
- Ciardi, D. R., Fabrycky, D. C., Ford, E. B., et al. 2013, *ApJ*, 763, 41, doi: [10.1088/0004-637X/763/1/41](https://doi.org/10.1088/0004-637X/763/1/41)
- Fabrycky, D. C., Lissauer, J. J., Ragozzine, D., et al. 2014, *ApJ*, 790, 146, doi: [10.1088/0004-637X/790/2/146](https://doi.org/10.1088/0004-637X/790/2/146)
- Fulton, B. J., & Petigura, E. A. 2018, *AJ*, 156, 264, doi: [10.3847/1538-3881/aae828](https://doi.org/10.3847/1538-3881/aae828)
- Fulton, B. J., Petigura, E. A., Howard, A. W., et al. 2017, *AJ*, 154, 109, doi: [10.3847/1538-3881/aa80eb](https://doi.org/10.3847/1538-3881/aa80eb)
- Furlan, E., Ciardi, D. R., Everett, M. E., et al. 2017, *AJ*, 153, 71, doi: [10.3847/1538-3881/153/2/71](https://doi.org/10.3847/1538-3881/153/2/71)
- Gaia Collaboration, Brown, A. G. A., Vallenari, A., et al. 2018, *A&A*, 616, A1, doi: [10.1051/0004-6361/201833051](https://doi.org/10.1051/0004-6361/201833051)
- Ginzburg, S., Schlichting, H. E., & Sari, R. 2018, *MNRAS*, 476, 759, doi: [10.1093/mnras/sty290](https://doi.org/10.1093/mnras/sty290)
- Gupta, A., & Schlichting, H. E. 2019, *MNRAS*, 487, 24, doi: [10.1093/mnras/stz1230](https://doi.org/10.1093/mnras/stz1230)
- . 2020, *MNRAS*, 493, 792, doi: [10.1093/mnras/staa315](https://doi.org/10.1093/mnras/staa315)
- He, M. Y., Ford, E. B., & Ragozzine, D. 2019, *MNRAS*, 490, 4575, doi: [10.1093/mnras/stz2869](https://doi.org/10.1093/mnras/stz2869)
- He, M. Y., Ford, E. B., Ragozzine, D., & Carrera, D. 2020, *AJ*, 160, 276, doi: [10.3847/1538-3881/abba18](https://doi.org/10.3847/1538-3881/abba18)
- Jin, S., Mordasini, C., Parmentier, V., et al. 2014, *ApJ*, 795, 65, doi: [10.1088/0004-637X/795/1/65](https://doi.org/10.1088/0004-637X/795/1/65)
- Kipping, D. 2018, *MNRAS*, 473, 784, doi: [10.1093/mnras/stx2383](https://doi.org/10.1093/mnras/stx2383)
- Lissauer, J. J., Ragozzine, D., Fabrycky, D. C., et al. 2011, *ApJS*, 197, 8, doi: [10.1088/0067-0049/197/1/8](https://doi.org/10.1088/0067-0049/197/1/8)
- Lissauer, J. J., Marcy, G. W., Bryson, S. T., et al. 2014, *ApJ*, 784, 44, doi: [10.1088/0004-637X/784/1/44](https://doi.org/10.1088/0004-637X/784/1/44)
- Lopez, E. D., & Fortney, J. J. 2013, *ApJ*, 776, 2, doi: [10.1088/0004-637X/776/1/2](https://doi.org/10.1088/0004-637X/776/1/2)
- . 2014, *ApJ*, 792, 1, doi: [10.1088/0004-637X/792/1/1](https://doi.org/10.1088/0004-637X/792/1/1)
- Mathur, S., Huber, D., Batalha, N. M., et al. 2017, *ApJS*, 229, 30, doi: [10.3847/1538-4365/229/2/30](https://doi.org/10.3847/1538-4365/229/2/30)
- Millholland, S. 2019, *ApJ*, 886, 72, doi: [10.3847/1538-4357/ab4c3f](https://doi.org/10.3847/1538-4357/ab4c3f)
- Millholland, S., Wang, S., & Laughlin, G. 2017, *ApJL*, 849, L33, doi: [10.3847/2041-8213/aa9714](https://doi.org/10.3847/2041-8213/aa9714)
- Mishra, L., Alibert, Y., Leleu, A., et al. 2021, arXiv e-prints, arXiv:2105.12745. <https://arxiv.org/abs/2105.12745>
- Murchikova, L., & Tremaine, S. 2020, *AJ*, 160, 160, doi: [10.3847/1538-3881/abab9e](https://doi.org/10.3847/1538-3881/abab9e)
- Owen, J. E., & Wu, Y. 2013, *ApJ*, 775, 105, doi: [10.1088/0004-637X/775/2/105](https://doi.org/10.1088/0004-637X/775/2/105)
- . 2017, *ApJ*, 847, 29, doi: [10.3847/1538-4357/aa890a](https://doi.org/10.3847/1538-4357/aa890a)
- Petigura, E. A. 2020, *AJ*, 160, 89, doi: [10.3847/1538-3881/ab9fff](https://doi.org/10.3847/1538-3881/ab9fff)
- Rogers, J. G., & Owen, J. E. 2021, *MNRAS*, 503, 1526, doi: [10.1093/mnras/stab529](https://doi.org/10.1093/mnras/stab529)
- Rogers, L. A. 2015, *ApJ*, 801, 41, doi: [10.1088/0004-637X/801/1/41](https://doi.org/10.1088/0004-637X/801/1/41)
- Rowe, J. F., Bryson, S. T., Marcy, G. W., et al. 2014, *ApJ*, 784, 45, doi: [10.1088/0004-637X/784/1/45](https://doi.org/10.1088/0004-637X/784/1/45)
- Van Eylen, V., Agentoft, C., Lundkvist, M. S., et al. 2018, *MNRAS*, 479, 4786, doi: [10.1093/mnras/sty1783](https://doi.org/10.1093/mnras/sty1783)
- Weiss, L. M., Millholland, S. C., Petigura, E. A., et al. 2021, *Protostars and Planets VII*, submitted
- Weiss, L. M., & Petigura, E. A. 2020, *ApJL*, 893, L1, doi: [10.3847/2041-8213/ab7c69](https://doi.org/10.3847/2041-8213/ab7c69)
- Weiss, L. M., Marcy, G. W., Petigura, E. A., et al. 2018, *AJ*, 155, 48, doi: [10.3847/1538-3881/aa9ff6](https://doi.org/10.3847/1538-3881/aa9ff6)
- Wolfgang, A., & Lopez, E. 2015, *ApJ*, 806, 183, doi: [10.1088/0004-637X/806/2/183](https://doi.org/10.1088/0004-637X/806/2/183)
- Zhu, W. 2020, *AJ*, 159, 188, doi: [10.3847/1538-3881/ab7814](https://doi.org/10.3847/1538-3881/ab7814)